ACS OMEGA

Open Access

http://pubs.acs.org/journal/acsodf

Article

Effect of Mn Doped on Structural, Optical, and Dielectric Properties of $BiFe_{1-x}Mn_xO_3$ for Efficient Antioxidant Activity

Muhammad Uzair, Shamsa Kanwal, Muhammad Iftikhar Khan, Wajeehah Shahid,* Badriah S. Almutairi, Muhammad Amin, Nawal Ansar, Samiah Shahid, and Jeong Ryeol Choi*

Cite This: *ACS Omega* 2023, 8, 42390−42397

Read Online

ACCESS | Metrics & More | Article Recommendations

ABSTRACT: Manganese-doped bismuth ferrites were synthesized using the coprecipitation method with the green extract *Azadirachta indica*. Our incorporation of the transition element, manganese, into bismuth ferrites tackles the challenge of increased leakage current often observed in intrinsic bismuth ferrites. We gained key insights through a comprehensive examination of the structural, dielectric, and optical properties of these materials, utilizing Fourier transform infrared spectroscopy (FTIR), impedance spectroscopy, and UV−visible spectroscopy, respectively. The formation of an octahedral geometry was confirmed using the FTIR technique. UV−visible spectroscopy indicated that 2% Mn doping is optimal, while we obtained a low band gap energy (2.21 eV) and high refractive index (3.010) at this amount of doping. The manufactured materials exhibited the typical ferrite-like dielectric response, that is, the dielectric parameter gradually decreased as the frequency increased and then stayed constant in the high-frequency range. Using the diphenylpicrylhydrazyl (DPPH) free radical assay, we also examined the antioxidant activity of bismuth ferrites. We concluded that among different Mn-doped $BiFeMnO_3$-based nanomaterials, the 2 wt % Mn-doped $BiFeMnO_3$ shows the highest antioxidant activity. This finding substantiates the efficacy of the optimized material with regard to its potent antioxidant activity, positioning it as a promising candidate for potential biomedical applications.

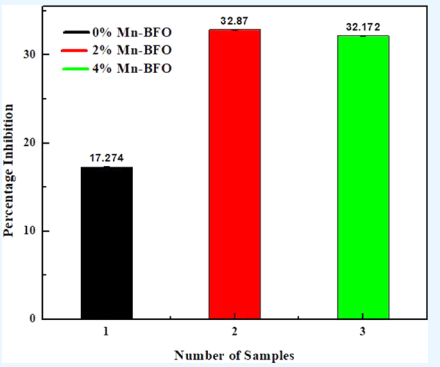

1. INTRODUCTION

Ferrites have drawn the attention of researchers due to their significance in various technological applications including optoelectronics with microwave and radio frequencies.[1] The most vital aspect of research along this line is the fabrication of required novel materials.[2] Among numerous transition metals, ferrites (iron oxide compounds) are an essential class of semiconductors that can be favorably used in ceramic coatings for solar cells, actuators, transformer cores, sensors, multistate memories, optoelectronic devices, and magnetic storage media.[3−5] Ferrites have been actively explored in connection with their potential applications in clay capacitors, drug delivery, computer technology, powerful arbitrary access memory, transducers, ferro fluids, high-density information storage, and cancer therapy.[6−12] Bismuth ferrite, which is a compound with the chemical formula $BiFeO_3$ (BFO), is one of the multiferroic materials at ambient temperature. To promote applications of bismuth ferrites in a variety of devices, it is necessary to improve their properties in a way that they have a dielectric loss, formation of an impurity phase, and a high leakage current.[13,14] It has been demonstrated that replacement at the A-site and B-site is a successful approach for decreasing dielectric loss and leakage current. Altering temperature and reaction time, pH, particle size, and cation distribution in sublattices and dopant substitution have all had a major influence on their dielectric, structural, and optical properties.[15,16] In multiferrites, these properties can be achieved by choosing an appropriate synthesis method. Multiferrites are often manufactured using hydrothermal, microwave combustion, ball milling, autocombustion, sol−gel, and coprecipitation processes.[17−20]

Antioxidants are known as chemical compounds that have properties that prevent, inhibit, or regulate the oxidation of a substrate. The compound could be either organic or inorganic. The base is termed an oxidizable base. Definitions of antioxidants, however, changed depending on their uses. In food science, the word "antioxidant" is implicitly restricted to compounds that block free lipid radical chains. However, the widespread presence of free radicals necessitates a more detailed, inclusive, and broadly recognized description. According to Halliwell (1990, 1995), an antioxidant is "any

Received: July 2, 2023
Revised: September 24, 2023
Accepted: September 29, 2023
Published: October 31, 2023

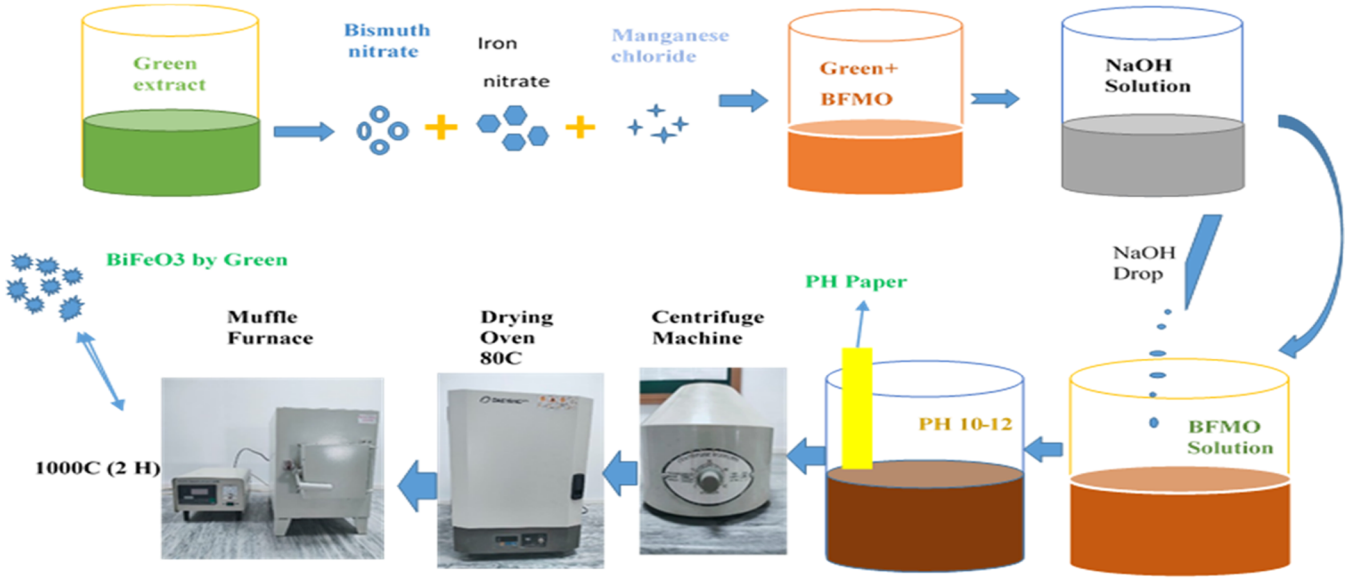

Figure 1. Fabrication of Mn-doped BFO.

substance present at low concentrations compared to those of an oxidizable substrate and significantly retards or prevents oxidation of that substrate." The substrate can be potentially oxidized when obtained from in vivo or in vitro systems. However, the concept and action of antioxidants were initially described by in vitro investigations. Thus, antioxidants in food science have been modified in light of the characteristics of the substrate and antioxidant itself. The oxidation of food components is inhibited, delayed, or controlled by chemicals present in foods in relatively small amounts. This prevents food spoiling and increases the shelf life. Oxidation was delayed as a result of the oxidation inhibition. The delay in the oxidation process thus extends the shelf life of foods. They are divided into primary antioxidants and secondary antioxidants. Based on how antioxidants work, this classification was developed. For instance, the main antioxidants neutralize free radicals either by a single electron transfer (SET) mechanism or by donating an H atom (hydrogen atom transfer, abbreviated as HAT). To effectively neutralize a large number of free radicals, these antioxidants are typically needed only in minimal amounts. One major factor contributing to these antioxidants' variety in nature is their high catalytic capabilities. Antioxidants that are phenolics fall into this category. These antioxidants can be quickly produced again. The process of neutralizing pro-oxidant catalysts has been used to describe secondary antioxidants. Examples include substances such as ethylenediaminetetraacetic acid (EDTA) and citric acid (CA) that act as chelators for pro-oxidant metal ions (such as Fe and Cu). Reactive substances like singlet oxygen may be neutralized by secondary antioxidants like carotene. These antioxidants typically only neutralize one free radical, making them quickly deplete.[21]

A lot of research is being done to produce properly doped BFO materials utilizing a variety of processes in order to achieve the necessary results. For example, Mn-doped BFO has a relatively high resistivity, higher dielectric constant, lower leakage current, and lower dielectric loss.[22,23] Pure BFO codoped with Mn and In, known to reduce leakage current, was also examined.[24] Due to its several benefits, including production of ultrafine particles with a tiny size in a relatively brief period of time at very low temperature and allowance of flexible stoichiometric control, the coprecipitation technique has drawn interest from many researches in fabricating nanosize ferrites. The Mn dopant was preferred due to its smaller size and greater stability. The increased surface-to-volume ratio of nanoparticles contributes to their antioxidant activity.[25] Compared to bulk materials, studies on Fe_2O_4 and $CoFe_2O_4$ indicated their higher antioxidant activity.[26,27]

Considerable research has been dedicated to generating appropriately doped BFO (bismuth ferrite) materials through various techniques; however, a research gap exists concerning the antioxidant activity of Mn-doped BFO materials.[28] The literature also lacks an exploration of the relationship between Mn doping in BFO synthesized by *Azadirachta indica* and its antioxidant properties. Motivated by this lack, we try to delve into their novel aspect beyond conventional electrical and structural characteristics. This study seeks to address this gap by systematically examining the antioxidant activity of Mn-doped BFO materials, potentially yielding broader applications beyond traditional uses as antioxidants find importance in biomedicine and materials science for combating oxidative stress. Furthermore, the study's outcomes could pave the way for multifunctional Mn-doped BFO materials with combined electrical, optical, dielectric, and antioxidant properties, inspiring innovations in electronics, sensors, and catalysis, where diverse material properties are sought after.

2. EXPERIMENTAL SECTION

The given chemicals were used in the fabrication of $BiFe_{1-x}Mn_xO_3$ multiferroic: bismuth nitrate ($Bi(NO_3)_3 \cdot 5H_2O$), manganese chloride ($MnCl_2$), iron nitrate ($Fe(NO_3)_3 \cdot 9H_2O$), sodium hydroxide (NaOH), distilled water, and ethanol.

2.1. Methodology. *A. indica*, iron nitrate, manganese chloride, and bismuth nitrate were used to synthesize Mn-doped bismuth ferrite nanoparticles using the coprecipitation technique. All chemicals were purchased from Fisher with 99.99% purity except *A. indica*. Fresh *A. indica* was obtained from the field of the Lahore region in Pakistan. *A. indica* was washed several times with water and ethanol to remove

https://doi.org/10.1021/acsomega.3c04714
ACS Omega 2023, 8, 42390−42397

unwanted ingredients from it. 40 g of *A. indica* leaves was first mixed with 200 mL of distilled water, and the combination was subsequently heated on a hot plate to 100 °C for 60 min. A fine greenish solution was obtained after filtering. This solution is the bioactive extract that houses compounds such as polyphenols and flavonoids, acting as reducing agents and stabilizers for nanoparticle formation. Gradually introduced to metal salt solutions under controlled conditions, the extract's compounds initiate metal ion reduction, fostering nucleation and small cluster formation. These nuclei enlarge as more metal atoms are reduced and deposited with manganese ions incorporating into the growing BFO crystal lattice. To maintain the pH 10−12, sodium hydroxide solution was gradually added under constant stirring. Achieving desired nanoparticle size and morphology, nanoparticles are heated at 1000 °C in a muffle furnace for 2 h, promoting crystallization, eliminating residual organics, and enhancing structural integrity. Throughout annealing, nanoparticles experience further crystalline growth, assimilating manganese ions into the BFO lattice and culminating in Mn-doped bismuth ferrite nanoparticle formation.

The synthesized nanoparticles are then characterized using FTIR (model), UV−vis spectroscopy (model), and impedance spectroscopy (model) to assess their structural, optical, and dielectric properties. The schematic view of the synthesis process is shown in Figure 1.

3. RESULTS AND DISCUSSION

3.1. Fourier Transform Infrared Spectroscopy (FTIR). The FTIR spectra of $BiFe_{1-x}Mn_xO_3$ nanostructures with x = 0, 2, and 4%, synthesized at 1000 °C for 2 h in the range of 500 to 2500 cm^{-1}, are presented in Figure 2. Metal oxide

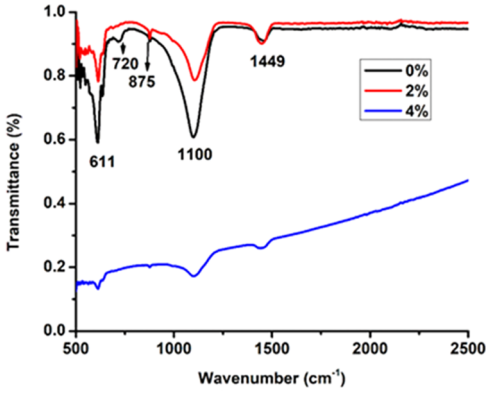

Figure 2. FTIR of $BiFe_{1-x}Mn_xO_3$ (x = 0, 2, 4%).

interactions such as Mn−O, Fe−O, and Bi−O are related to absorption peaks ranging from 500 to 1500 cm^{-1}[29] The absorption bands at 611 and 875 cm^{-1} are associated with Fe−O stretching vibrations.[12] The small bands appeared at 720 cm^{-1} interconnected with O−Fe−O vibrations, which demonstrates the octahedral geometry of the FeO_6 group in perovskite materials; therefore, all samples have perovskite structures.[30,31] The absorption peaks observed at 1100 and 1449 cm^{-1} are interlinked with C═C and C═O stretching vibrations, respectively.[32] The broad absorption spectra at 1100 cm^{-1} indicate bending vibrations of nitrate (NO_3^-) ions, and these bands vanish as the concentration of the Mn dopant increases. The formation of oxygen gaps in the samples is produced by the disappearance of Fe−O vibrations at 720 cm^{-1} and the replacement of this band by hole valleys at 875 cm^{-1} as the concentration of Mn increases.[33]

3.2. UV−Visible Spectroscopy. UV−visible spectroscopy of the prepared bismuth ferrites is illustrated in the Tauc plot. The formula shown below can be used to calculate the band gap measurements of all prepared samples.[34]

$$\alpha h\nu = B(h\nu - E_g)^n \quad (1)$$

Here, E_g, B, $h\nu$, and α are the energy band gap, absorption edge width parameter, incident photon energy, and absorption coefficient respectively, whereas n is an exponent value dependent on indirect (2) and direct transition (1/2), across the energy band gap.[35] The variation in band gap values resulting from Mn doping in bismuth ferrites signifies a significant interplay in optical characteristics, as shown in Figure 3. The observed decrease in energy band gaps with

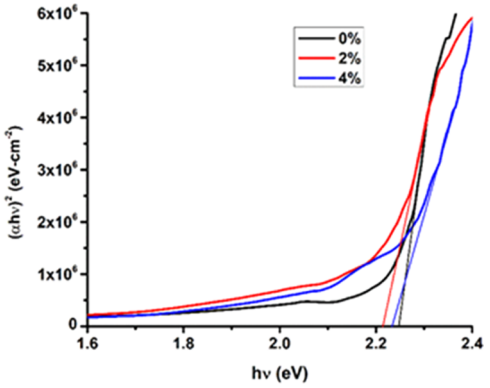

Figure 3. Band gap energy of $BiFe_{1-x}Mn_xO_3$ (x = 0, 2, 4%).

increasing Mn concentration (2.29 → 2.21 → 2.25 eV for x = 0, 2, 4%, respectively) stems from the intricate interplay of crystalline size alterations and the introduction of defect-induced energy levels near the conduction band. This band gap reduction, in turn, enhances the material's capability to facilitate charge transfer and electron mobility. This better charge transport capability as a result of the lower energy barrier may improve the device performance. A promising method for improving material characteristics and producing enhanced functional materials for many applications is the targeted regulation of the band gap using Mn doping.[33,36]

3.3. Dielectric Constant. The dielectric constant was plotted against the frequency in Figure 4 in order to investigate the frequency-dependent dielectric dispersion of Mn-doped bismuth ferrites. To compute the dielectric constant of each composition, we used the following equation[32]

$$\varepsilon' = \frac{(C_P d)}{\varepsilon_o A} \quad (2)$$

where ε' is the dielectric constant, d is the thickness of plate, ε_o is the electric permittivity of the free space, C_P is the parallel capacitance derived through an impedance analyzer, and A is the cross-sectional area of the plate. In all concentrations (x = 0, 2, 4%), the dielectric measurement of the samples exhibits consistent behavior, providing crucial insights into the material's electrical properties. The dielectric constant decreases and becomes more significant as the frequency becomes higher. Specifically, the dielectric constant exhibits a pattern of increasing with temperature and loss, and this trend

https://doi.org/10.1021/acsomega.3c04714
ACS Omega 2023, 8, 42390−42397

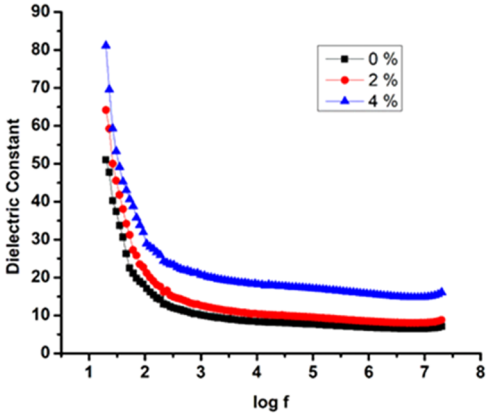

Figure 4. Dielectric constant of $BiFe_{1-x}Mn_xO_3$ (x = 0, 2, 4%).

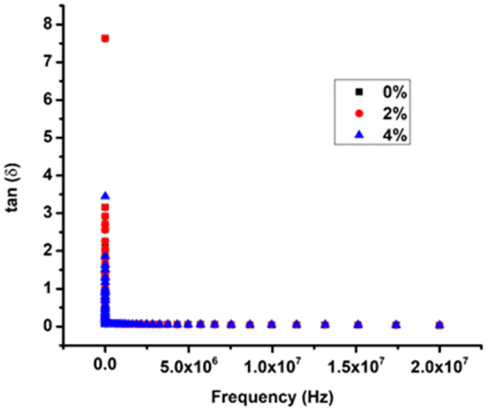

Figure 5. Tangent loss vs frequency for $BiFe_{1-x}Mn_xO_3$ (x = 0, 2, 4%).

is more pronounced at higher frequencies. This phenomenon is attributed to the carriers taking time to align with the direction of the electric field. At elevated frequencies, the rapid rotation of the field prevents carriers from reorienting themselves to match the field direction. It is noteworthy that all three samples exhibit characteristic ferrite behavior, where the dielectric constant starts at high values in the low-frequency range and decreases as frequency increases, eventually stabilizing at higher frequencies.[37,38] Highly resistive grain borders and highly conducting grains make up a polycrystalline material. Highly resistive grain boundaries are active in the low-frequency range, preventing conduction and producing a high value for the dielectric constant. However, in the high-frequency regime, low resistive or strongly conducting grains start to become active, which causes conduction and a low value for the dielectric constant. High-resistance grain boundaries (no conduction) become active and increase at low frequencies. Low-resistive grains become active at high frequencies, leading to the electric conduction being increased.[39]

3.3.1. Tangent Loss. Tangent loss ($\tan\delta$) refers to the dissipation of energy in dielectrics. Tangent losses in materials are, in general, caused by imperfections, impurities, and defects in the crystal lattice, where these losses make polarization lag behind the applied external field. The numerical value of $\tan\delta$ for each sample was computed using the equation[32]

$$\tan\delta = \frac{1}{(2\pi f C_P R_P)} \tag{3}$$

where R_P is the parallel resistance, C_P is the parallel capacitance, f is the frequency, and δ is the loss angle. According to the Maxwell–Wagner model of polarization together with Koop's phenomenological theory, energy loss and dielectric constant are almost independent of frequency at higher frequencies.[40] This phenomenon implies that polarization in any polycrystalline material is brought on by well-conducting grains spaced apart by weak grain boundaries. Space charges may follow the applied field because of their longer relaxation times at lower frequencies, but because they lag the applied field at higher frequencies, they are unable to rest. Tangent loss and dielectric constant both increase with increasing Mn concentrations at lower frequencies; however, at higher frequencies, both exhibited frequency independent behavior. Figure 5 depicts the tangent loss plotted against frequency. At high frequencies of 5–50 kHz, especially between 5 and 10 kHz, the tangent loss increases as the dopant concentration increases from x = 0.05 to 0.1. Both the dielectric constant and tangent loss exhibit conventional ferrite behaviors, i.e., they decrease with increasing frequency. On the other hand, tangent loss increases with increasing doping concentration of manganese.[41,42]

3.3.2. Concentration. Figure 6 describes the fluctuations of the dielectric constant (ε') with concentration. By increasing

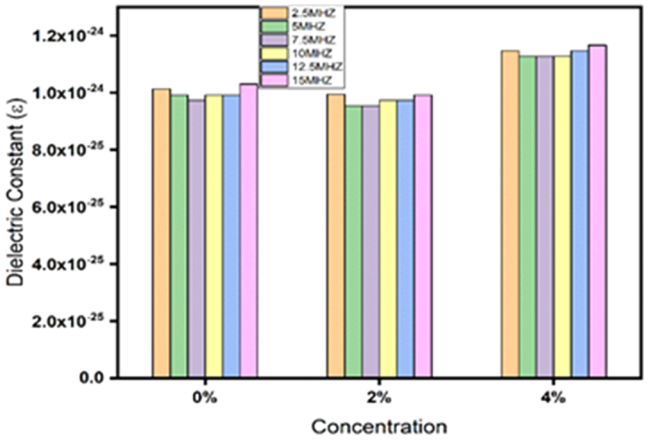

Figure 6. Dielectric constant vs concentration of $BiFe_{1-x}Mn_xO_3$ (x = 0, 2, 4%).

the concentration of all samples, the dielectric constant is enhanced. The increase in sample porosity and reduction in particle size with an increasing concentration can both be used to describe the dispersion in the dielectric constant for all samples. The result is a surface area with a high resistive nature, which causes the grain boundary region being expanded, while the contact with neighboring grains contracts. More structural defects are introduced as a result of the accumulation of charge carriers at the interface caused by the grain boundaries and increased porosity. The effects of Mn doping and increasing number of grain boundaries have been associated with structural variations and enhanced dielectric values.[43,44]

3.3.3. Refractive Index. The optical refractive index (n_r) of bismuth ferrites is given by[45]

$$n_r = \frac{1+R}{1-R} + \sqrt{\frac{4R}{(1-R)^2} - k^2} \tag{4}$$

https://doi.org/10.1021/acsomega.3c04714
ACS Omega 2023, 8, 42390−42397

where R is the reflectance and k is the extinction coefficient that will be defined later. This equation was used to calculate the reflectance spectrum of bismuth ferrites having concentrations of x = 0, 2, and 4%. The corresponding results are depicted in Figure 7. These observed values clearly show how

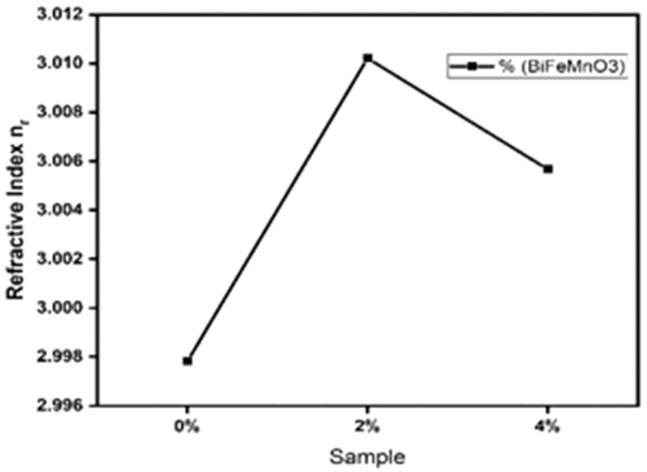

Figure 7. Refractive index of $BiFe_{1-x}Mn_xO_3$ (x = 0, 2, 4%).

the Mn content affects the refractive index of bismuth ferrites. A noticeable pattern develops when more Mn is incorporated into the ferrite structure: a rise in Mn concentration is accompanied by an increase in the refractive index. The interaction between Mn dopants and the crystal structure of bismuth ferrites is responsible for this phenomenon. Mn ions cause the atomic structure to be disturbed, which changes the electronic energy levels and produces local field effects. As a result, the refractive index is impacted, rising as the Mn concentration increases. With the given values, the refractive index clearly increases from 2.998 at x = 0 to 3.010 at x = 2% and further to 3.005 at x = 4% (Figure 8).[46,47]

3.3.4. Extinction Coefficient. The extinction coefficient k of bismuth ferrites is represented as[45]

$$k = \frac{\alpha\lambda}{4\pi} \tag{5}$$

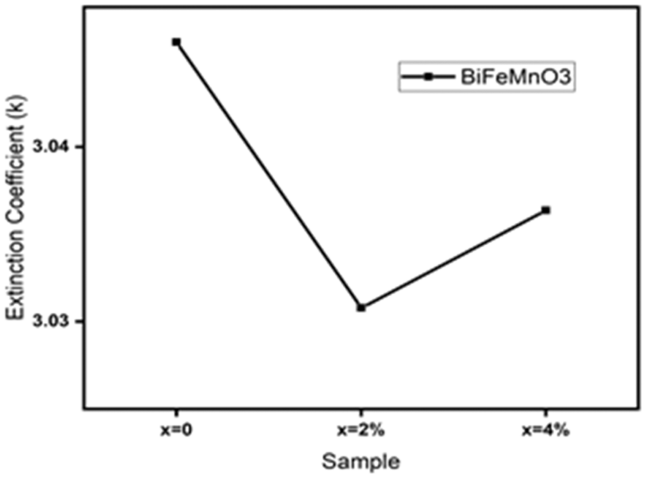

Figure 8. Plot of the extinction coefficient of $BiFe_{1-x}Mn_xO_3$ (x = 0, 2, 4%).

This equation was used to compute the absorption spectrum of bismuth ferrites having concentrations x = 0, 2, and 4%, that is, by using the extinction coefficient k, it is possible to estimate the amount of absorption loss associated with electromagnetic wave propagation. The corresponding computation is shown in Figure 9. We can confirm from this figure that the extinction

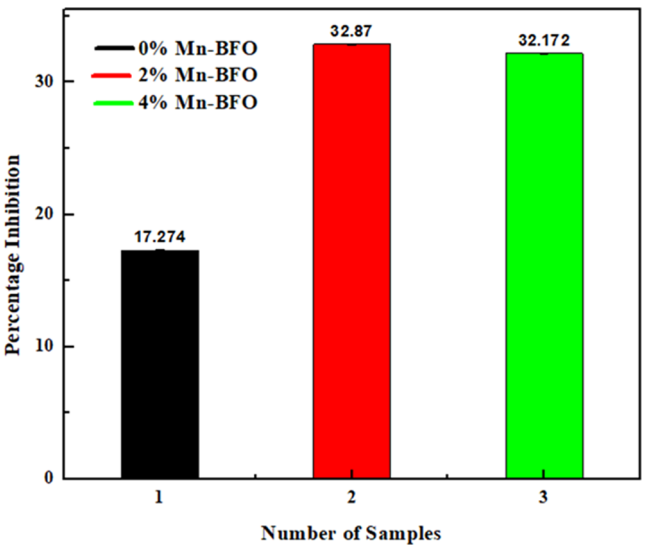

Figure 9. Graph b/w number of sample percentage inhibition of $BiFe_{1-x}Mn_xO_3$ (x = 0, 2, 4%).

coefficients of the pure and Mn-doped bismuth ferrites are 3.045, 3.030, and 3.036 in turn. The extinction coefficient decreases as the Mn concentration increases, demonstrating that the quality of bismuth ferrites is directly interrelated with reduced optical losses through absorption.

3.4. Antioxidant Activity. The antioxidant activity of the samples was determined by using the 2,2-diphenyl-1-picrylhydrazyl (DPPH) radical, implementing a slightly modified method described in ref 48. Antioxidant action of a phenolic compound can be explained on the basis of a HAT mechanism or a single-electron mechanism. In HAT, a free radical and an antioxidant with a H atom, represented by AH, interact with each other. While the antioxidant is changed to an antioxidant free radical (A*), the free radical is stabilized and becomes a neutral species. The phenolic antioxidant (AH) can give the free radical substrate, a H atom, in exchange as well as an antioxidant free radical (A*), forming a nonradical substrate (RH, ROH, or ROOH) species:[49] this process can be represented as

$$R^{\bullet} + AH \rightarrow RH + A^{\bullet}$$
$$RO^{\bullet} + AH \rightarrow ROH + A^{\bullet}$$
$$ROO^{\bullet} + AH \rightarrow ROOH + A^{\bullet}$$
$$RO^{\bullet} + A^{\bullet} \rightarrow ROA$$
$$ROO^{\bullet} + A^{\bullet} \rightarrow ROOA \tag{6}$$

The reduction potential explains why an antioxidant gives up one atom of hydrogen. Shahidi and Ambigaipalan (2015) indicated, in relation with this, that "unless the reaction is kinetically infeasible, any compound that has a reduction potential lower than that of a free radical (or oxidized species) is capable of donating its hydrogen atom to that of the free

https://doi.org/10.1021/acsomega.3c04714
ACS Omega 2023, 8, 42390−42397

radical." Using the following formula, the percentage inhibition activity of the samples and standard was calculated.

$$\text{percentage inhibition} = \frac{(A_1 - A_2)}{A_1} \times 100 \quad (7)$$

A_1 = absorbance value of the control.

A_2 = absorbance value of samples.

The antioxidant activity of the samples was determined by their DPPH radical scavenging activity, which is explained in Table 1.

Table 1. Percentage Inhibition of Mn-BFO (x = 0, 2, and 4%)

sr. no.	samples	percentage Inhibition
1.	BFO (0)	17.24 ± 0.054
2.	BFO (2%)	32.18 ± 0.12
3.	BFO (4%)	32.87 ± 0.044

Values are expressed as mean ± standard deviation when n = 5. The impressive percentage suppression of DPPH radical scavenging activity in 5 wt % Mn-doped $BiFeMnO_3$ is demonstrated in Figure 9, which also highlights the material's substantial antioxidant potential. Notably, BFO (x = 0%) showed a 17.24% percentage inhibition, whereas BFO (2%) and BFO (4%) showed higher inhibitions of 32.18 and 32.87%, respectively. This information highlights the substance's potency in scavenging free radicals, an essential property in the fight against oxidative stress-related disorders. The synergistic effect of manganese incorporation and the intrinsic antioxidant characteristics of the bismuth ferrite matrix is responsible for the improved DPPH radical scavenging activity of the 5 wt % Mn-doped $BiFeMnO_3$. Manganese is a transition metal that exhibits redox activity, allowing it to participate in catalytic processes that neutralize free radicals. Bismuth ferrites have a unique crystal structure and electrical arrangement that further enhance their ability to scavenge radicals. This exceptional antioxidant activity enables applications in biomedicine. In biomedical applications, a material's ability to resist oxidative stress is essential for preventing cellular damage and maintaining overall health. The 5 wt % Mn-doped $BiFeMnO_3$ demonstrates excellent antioxidant effectiveness, making it a suitable choice for therapeutic interventions focused at diseases associated with oxidative stress. Its numerous advantageous traits, which combine enhanced electron mobility and effective radical scavenging, offer hope for extending biomedical applications and assisting in the development of cutting-edge antioxidant-based technologies.

4. CONCLUSIONS

In this study, a Mn-doped $BiFe_2O_3$ was successfully synthesized using the coprecipitation method with the assistance of a green extract, *A. indica*. Fourier transform infrared spectroscopy (FTIR) analysis revealed distinct metal oxide interactions involving Mn−O, Fe−O, and Bi−O bonds within the 500−1500 cm^{-1} range. This confirmed the successful formation of Mn-doped $BiFe_2O_3$ (Mn-BFO). A low band gap energy (2.21 eV) and high refractive index are observed at 2% of Mn-doped BFO, which is due to different ionic radii of host and doped atoms. The inverse relation between the refractive index and extinction coefficient is observed by Mn doping. The 2% Mn-$BiFe_2O_3$ has good dielectric characteristics as compared to others. The antioxidant activity results obtained using *A. indica* showed that Mn-doped $BiFeMnO_3$ nanomaterials were highly efficient. Especially, among all samples, 2 wt % Mn-doped $BiFeMnO_3$ demonstrated excellent antioxidant activity and can be used for biomedical applications.

AUTHOR INFORMATION

Corresponding Authors

Wajeehah Shahid − *Department of Physics, The University of Lahore, Lahore 53700, Pakistan*; orcid.org/0000-0002-8871-6534; Email: Wajeeha.shahid@phys.uol.edu.pk

Jeong Ryeol Choi − *School of Electronic Engineering, Kyonggi University, Suwon, Gyeonggi-do 16227, Republic of Korea*; Email: choiardor@hanmail.net

Authors

Muhammad Uzair − *Department of Physics, The University of Lahore, Lahore 53700, Pakistan*

Shamsa Kanwal − *Department of Physics, The University of Lahore, Lahore 53700, Pakistan*

Muhammad Iftikhar Khan − *Department of Physics, The University of Lahore, Lahore 53700, Pakistan*

Badriah S. Almutairi − *Department of Physics, College of Science, Princess Nourah bint Abdulrahman University, Riyadh 11671, Saudi Arabia*

Muhammad Amin − *Department of Physics, The University of Lahore, Lahore 53700, Pakistan*

Nawal Ansar − *Department of Physics, The University of Lahore, Lahore 53700, Pakistan*

Samiah Shahid − *Institute of Molecular Biology and Biotechnology, The University of Lahore, Lahore 54000, Pakistan*

Complete contact information is available at: https://pubs.acs.org/10.1021/acsomega.3c04714

Notes

The authors declare no competing financial interest.

The complete mailing address information for Princess Nourah bint Abdulrahman University is: Department of Physics, College of Science, Princess Nourah bint Abdulrahman University, P.O. Box 84428, Riyadh 11671, Saudi Arabia.

ACKNOWLEDGMENTS

This research was supported by the Princess Nourah bint Abdulrahman University Researchers Supporting Project number (PNURSP2023R327), Princess Nourah bint Abdulrahman University, Riyadh, Saudi Arabia. This work was supported by the National Research Foundation of Korea (NRF) grant funded by the Korea government (MSIT) (No.: NRF-2021R1F1A1062849).

REFERENCES

(1) Azim, M.; Chaudhry, M. A.; Amin, N.; et al. Structural and optical properties of cr-substituted co-ferrite synthesis by coprecipitation method. *Dig. J. Nanomater. Bio Struct.* **2016**, *11*, 953−962.

(2) Chandrika, M.; Ravindra, A. V.; Rajesh, C.; et al. Studies on structural and optical properties of nano $ZnFe_2O_4$ and $ZnFe_2O_4$-TiO_2 composite synthesized by co-precipitation route. *Mater. Chem. Phys.* **2019**, *230*, 107−113.

(3) Pashchanka, M.; Hoffmann, R. C.; Schneider, J. J. In *Template-directed Formation Of Polycrystalline Magnesium Oxide Nanorods,*

https://doi.org/10.1021/acsomega.3c04714
ACS Omega 2023, 8, 42390−42397

Physics, Chemistry and Application of Nanostructures; World Scientific, 2009; pp 373−376.
(4) Qin, D.; Li, H. Fabrication and magnetic properties of $Fe_{0.3}Co_{0.7}$ nanowires arrays. *Chin. J. Mater. Res.* **2007**, *21* (5), 501−505.
(5) Ghahfarokhi, S. M.; Shobegar, E. M. Structural, magnetic, dielectric and optical properties of $Sr_{1-x}Mn_xFe_2O_4$ nanoparticles fabricated by sol-gel method. *J. Alloys Compd.* **2018**, *768*, 65−73.
(6) Hait, S.; Ghose, S.; Mandal, K. Effect of Ba and Y co-doping on the structural and magneto-electric properties of $BiFeO_3$ ceramic. *J. Alloys Compd.* **2020**, *822*, No. 153614.
(7) Bhoyar, D. N.; Somvanshi, S. B.; Kharat, P. B.; et al. Structural, infrared, magnetic and ferroelectric properties of $Sr_{0.5}Ba_{0.5}Ti_{1-x}Fe_xO_3$ nanoceramics: Modifications via trivalent Fe ion doping. *Phys. B* **2020**, *581*, No. 411944.
(8) Aslam, A.; Morley, N.; Amin, N.; et al. Study of structural, optical and electrical properties of La^{3+} doped $Mg_{0.25}Ni_{0.15}Cu_{0.25}Co_{0.35}Fe_{2-x}$ La_x O_4 spinel ferrites. *Phys. B* **2021**, *602*, No. 412565.
(9) Lv, L.; Wang, Y.; Cheng, P.; et al. Production of MFe_2O_4 (M= Zn, Ni, Cu, Co and Mn) multiple cavities microspheres with salt template to assemble a high-performance acetone gas sensor. *J. Alloys Compd.* **2022**, *904*, No. 164054.
(10) Kharat, P. B.; Somvanshi, S. B.; Somwanshi, S. B.; et al. Synthesis, characterization and hyperthermic evaluation of PEGylated superparamagnetic $MnFe_2O_4$ ferrite nanoparticles for cancer therapeutics applications. *Macromol. Symp.* **2021**, *400*, No. 2100130, DOI: 10.1002/masy.202100130.
(11) Maity, A.; Raychaudhuri, A. K.; Ghosh, B. High sensitivity NH_3 gas sensor with electrical readout made on paper with perovskite halide as sensor material. *Sci. Rep.* **2019**, *9* (1), No. 7777.
(12) Ahmed, I.; Mustafa, G.; Subhani, M. U.; et al. A detailed investigation of lanthanum substituted bismuth ferrite for enhanced structural, optical, dielectric, magnetic and ferroelectric properties. *Results Phys.* **2022**, *38*, No. 105584.
(13) Ataseven, T.; Tataroğlu, A. Temperature-dependent dielectric properties of $Au/Si_3N_4/n$-Si (metal—insulator—semiconductor) structures. *Chin. Phys. B* **2013**, *22* (11), No. 117310.
(14) Baqiah, H.; Talib, Z. A.; Shaari, A. H.; et al. Synthesis, optical and magnetic behavior of $(BiFeO_3)_{1-x}(\alpha\text{-}Fe_2O_3)$ x nanocomposites. *Mater. Sci. Eng. B* **2018**, *231*, 5−10.
(15) Mustafa, G.; Islam, M. U.; Zhang, W.; et al. Investigation of the Role of Ce^{3+} Substituted Ions on Dielectric Properties of Co-Cr Ferrites Prepared by Co-precipitation Method. *J. Electron. Mater.* **2016**, *45*, 5830−5838.
(16) Ahmad, I.; Ahmad, M.; Ali, I.; et al. Effects of Gd-substitutions on the microstructure, electrical and electromagnetic behavior of M-type hexagonal ferrites. *J. Electron. Mater.* **2015**, *44*, 2221−2229.
(17) Ikram, S.; Jacob, J.; Mehboob, K.; et al. Relationship of Various Structural Parameters with Magnetic Behavior of Stoichiometric Tb^{3+} and Dy^{3+} Co-substituted $NiFe_2O_4$ Nanostructures. *J. Supercond. Novel Magn.* **2021**, *34*, 1753−1758.
(18) Amin, N.; Arshad, M. I.; Ajaz-Un-Nabi, M.; et al. Effect Of Cd2 Ions Insertion On Structural, Optical And Electrical Properties Of Zn0.3co0.7-xcdxfe2o4 (0≤ X≤ 0.7) Ferrites. *J. Ovonic Res.* **2019**, *15* (1), 27−35.
(19) Mustafa, G.; Islam, M. U.; Zhang, W.; et al. Investigation of structural and magnetic properties of Ce^{3+}-substituted nanosized Co−Cr ferrites for a variety of applications. *J. Alloys Compd.* **2015**, *618*, 428−436.
(20) Zhang, X. Y.; Qi, X. W.; Qi, J. Q.; et al. Preparation and Properties of Multiferroic La-Doped $BiFeO_3$ Thin Film. *Adv. Mater. Res.* **2012**, *486*, 417−421.
(21) Dai, W.; Zhang, C.; Zhao, L.; et al. Effects of Cu content in Al-Cu alloys on microstructure, adhesive strength, and corrosion resistance of thick micro-arc oxidation coatings. *Mater. Today Commun.* **2022**, *33*, No. 104195.
(22) Varshney, D.; Kumar, A.; Verma, K. Effect of A site and B site doping on structural, thermal, and dielectric properties of $BiFeO_3$ ceramics. *J. Alloys Compd.* **2011**, *509* (33), 8421−8426.
(23) Amin, M.; Rafique, H. M.; Yousaf, M.; et al. Structural and impedance spectroscopic analysis of Sr/Mn modified $BiFeO_3$ multiferroics. *J. Mater. Sci.: Mater. Electron.* **2016**, *27*, 11003−11011.
(24) Arya, G. S.; Negi, N. Effect of In and Mn co-doping on structural, magnetic and dielectric properties of $BiFeO_3$ nanoparticles. *J. Phys. D: Appl. Phys.* **2013**, *46* (9), No. 095004.
(25) Das, D.; Nath, B. C.; Phukon, P.; et al. Synthesis and evaluation of antioxidant and antibacterial behavior of CuO nanoparticles. *Colloids Surf., B* **2013**, *101*, 430−433.
(26) Paul, S.; Saikia, J. P.; Samdarshi, S. K.; Konwar, B. K. Investigation of antioxidant property of iron oxide particlesby 1′-1′ diphenylpicryl-hydrazyle (DPPH) method. *J. Magn. Magn. Mater.* **2009**, *321* (21), 3621−3623.
(27) Covaliu, C. I.; Matei, C.; Litescu, S.; et al. Radical scavenger properties of oxide nanoparticles stabilized with biopolymer matrix. *Mater. Plast.* **2010**, *47* (1), 5−10.
(28) Zeb, A. Concept, mechanism, and applications of phenolic antioxidants in foods. *J. Food Biochem.* **2020**, *44* (9), No. e13394.
(29) Chen, P.; Xu, X.; Koenigsmann, C.; et al. Size-dependent infrared phonon modes and ferroelectric phase transition in $BiFeO_3$ nanoparticles. *Nano Lett.* **2010**, *10* (11), 4526−4532.
(30) Liu, T.; Xu, Y.; Feng, S.; et al. A facile route to the synthesis of $BiFeO_3$ at low temperature. *J. Am. Ceram. Soc.* **2011**, *94* (9), 3060−3063.
(31) Srivastav, S. K.; Gajbhiye, N. S. Low temperature synthesis, structural, optical and magnetic properties of bismuth ferrite nanoparticles. *J. Am. Ceram. Soc.* **2012**, *95* (11), 3678−3682.
(32) Vijayasundaram, S. V.; Suresh, G.; Kanagadurai, R. Synthesis, thermal, structural, and magnetic properties of phase-pure nanocrystalline $BiFeO_3$ via wet chemical route. *Appl. Phys. A* **2015**, *121*, 681−688.
(33) Ghahfarokhi, S. E. M.; Larki, M. R.; Kazeminezhad, I. The effect of Mn doped on the structural, magnetic, dielectric and optical properties of bismuth ferrite ($BiFe_{1-x}Mn_xO_3$) nanoparticles. *Vacuum* **2020**, *173*, No. 109143.
(34) Ramzan, A.; Naz, S.; Zubair, A.; et al. Raveling out the effect of Pr3+ ions substitution on different properties of nano-sized hexagonal ferrites. *Mater. Sci. Eng. B* **2023**, *297*, No. 116717.
(35) Makarovic, M.; Bayir, M. Ç.; Ursic, H.; et al. Domain wall conductivity as the origin of enhanced domain wall dynamics in polycrystalline $BiFeO_3$. *J. Appl. Phys.* **2020**, *128* (6), No. 064104, DOI: 10.1063/5.0017374.
(36) Khorrami, G. H.; Zak, A. K.; Kompany, A.; yousefi, R. Optical and structural properties of X-doped (X= Mn, Mg, and Zn) PZT nanoparticles by Kramers−Kronig and size strain plot methods. *Ceram. Int.* **2012**, *38* (7), 5683−5690.
(37) Das, S.; Senapati, S.; Pradhan, G. K.; et al. A Facile Microwave-Assisted Nanoflower-to-Nanosphere Morphology Tuning of $Cu\text{-}Se_{1-x}Te_{1+x}$ for Optoelectronic and Dielectric Applications. *ACS Appl. Nano Mater.* **2023**, *6* (7), 5298−5312.
(38) Sahoo, D.; Senapati, S.; Samal, S.; et al. Optical and Dielectric Characterization of Nanoparticle-Based $Cu_2Ni_{1+x}Sn_{1-x}S_4$ Nanosphere Synthesized by Facile Solvothermal Method. *ACS Appl. Eng. Mater.* **2023**, *1* (3), 1001−1012.
(39) Riaz, S.; Shah, S. M. H.; Akbar, A.; et al. Effect of Mn doping on structural, dielectric and magnetic properties of BiFeO 3 thin films. *J. Sol-Gel Sci. Technol.* **2015**, *74*, 329−339.
(40) Sharma, A. D.; Hemanta, H.; Sharma, H. B. Effect of Mn substitution on structural and dielectric properties of bismuth ferrite. *Ferroelectrics* **2017**, *519* (1), 187−193.
(41) Anjum, S.; Nazli, H.; Khurram, R.; et al. Role of Zn substitution on structural, magnetic and dielectric properties of Cu−Cr spinel ferrites. *Indian J. Phys.* **2016**, *90*, 869−880.
(42) Amin, M.; Rafique, H. M.; Mustafa, G. M.; et al. Effect of La/Cr co-doping on dielectric dispersion of phase pure $BiFeO_3$

https://doi.org/10.1021/acsomega.3c04714
ACS Omega 2023, 8, 42390−42397

nanoparticles for high frequency applications. *J. Mater. Res. Technol.* **2021**, *13*, 1534−1545.
(43) Lakshmi, C. S.; Sridhar, C. S. L. N.; Govindraj, G.; et al. Structural, magnetic and dielectric investigations in antimony doped nano-phased nickel-zinc ferrites. *Phys. B* **2015**, *459*, 97−104.
(44) Atiq, S.; Majeed, M.; Ahmad, A.; et al. Synthesis and investigation of structural, morphological, magnetic, dielectric and impedance spectroscopic characteristics of Ni-Zn ferrite nanoparticles. *Ceram. Int.* **2017**, *43* (2), 2486−2494.
(45) Venkateswarlu, A. R.; Varma, G.; Nath, R. Optical and electrical properties of spray pyrolysis deposited nano-crystalline $BiFeO_3$ films. *AIP Adv.* **2011**, *1* (4), No. 042140.
(46) Priyadarshini, P.; Alagarasan, D.; Ganesan, R.; et al. Influence of proton ion irradiation on the linear−nonlinear optoelectronic properties of $Sb_{40}Se_{20}S_{40}$ thin films at different fluences for photonic devices. *ACS Appl. Opt. Mater.* **2023**, *1* (1), 55−68.
(47) Priyadarshini, P.; Das, S.; Alagarasan, D.; et al. Role of Bismuth incorporation on the structural and optical properties in $Bi_xIn_{35-x}Se_{65}$ thin films for photonic applications. *J. Am. Ceram. Soc.* **2021**, *104* (11), 5803−5814.
(48) Yeo, J.; Shahidi, F. Revisiting DPPH (2, 2-diphenyl-1-picrylhydrazyl) assay as a useful tool in antioxidant evaluation: a new IC100 concept to address its limitations. *J. Food Bioact.* **2019**, *7*, 36−42, DOI: 10.31665/JFB.2019.7196.
(49) Santos-Sánchez, N. F.; Salas-Coronado, R.; Villanueva-Cañongo, C.; Hernández-Carlos, B. Antioxidant Compounds and Their Antioxidant Mechanism. In *Antioxidants*; IntechOpen, 2019; Vol. *10*, pp 1−29.

https://doi.org/10.1021/acsomega.3c04714
ACS Omega 2023, 8, 42390−42397